acta physica slovaca vol. 48 No. 4, 427 – 440 August 1998

CHARACTERIZATION OF SURFACES AND INTERFACES BY HARD X-RAY REFLECTOMETRY AND DIFFUSE SCATTERING AT GRAZING INCIDENCE[1]

M. Jergel[2], E. Majková, Š. Luby, R.Senderák
Institute of Physics, Slovak Academy of Sciences, Dúbravská cesta 9, 842 28 Bratislava, Slovakia

V.Holý
Laboratory of Thin Films and Nanostructures, Faculty of Science, Masaryk University, Kotlářská 2, 611 37 Brno, Czech Republic

Received 12 May 1998, accepted 28 July 1998

The techniques for characterization of surfaces and interfaces of mono/multilayer thin films based on measurements of the specular reflectivity and diffuse scattering at grazing incidence of hard X-rays are outlined. The specular reflectivity and interface diffuse scattering from a single interface are discussed within the Fresnel theory, the first Born approximation, and the first distorted-wave Born approximation. Their extension to the multilayer case is shown. The specular reflectivity gives basic structural parameters of a multilayer like the thicknesses of the individual layers and their fluctuations, the total multilayer thickness, the number of multilayer periods in a periodic multilayer, atomic densities of individual layers, and the parameter called "interface roughness" which characterizes the projection of an interface profile into the normal direction with respect to the multilayer surface. To distinguish between geometrically rough and compositionally graded interfaces, a mapping of the diffusely scattered X-ray intensity throughout the reciprocal space is inevitable which provides the interface parameters like the rms value of the real geometrical roughness, lateral correlation length, fractal dimension, as well as a degree of the vertical conformality of the interface profiles which reflects the growth mechanism. Some practical examples of such evaluations on amorphous W/Si multilayers are presented and the results discussed from the point of view of possible applications.

[1]Presented at The International Workshop on Diagnostics of Solid State Surfaces and Interfaces, Bratislava, 24 – 26 June 1998
[2]E-mail address: fyzijerm@savba.sk

1 Introduction

Rapid development of sophisticated deposition methods during the last two decades has stimulated preparation of new mono- and multilayer thin film structures for microelectronics, X-ray and UV optics, sensors and other applications. On the other hand, mesoscopic thin film structures exhibiting new cross-over and low-dimensional magnetic, electronic transport, and superconductivity effects represent a challenge for basic research.

Knowledge of an interconnection between the structure of a thin film and the properties of interest is a prerequisite for any optimization of application elements as well as for a proper understanding of basic physical phenomena unique for thin films. Among other new surface-sensitive experimental techniques developed recently to characterize thin films, those utilizing grazing incidence of hard X-rays are unique due to their non-destructive character and the ability to determine the relevant structural parameters over microscopic sample areas with high accuracy and within reasonably short times.

To increase the surface sensitivity and suppress the substrate signal, the grazing incidence (or exit) X-ray diffraction technique was developed in the in-plane (coplanar) and out-of-plane (non-coplanar) geometry to tailor the internal atomic structure of thin films or near-surface region. Here, the angle of incidence and/or exit is tuned near the critical angle for the total external reflection (TER) which is a few tenths of degree for hard X-rays. On the other hand, the X-ray specular reflectivity and interface diffuse (non-specular) scattering at grazing incidence provide an excellent tool to study surface/interface morphology independently of the internal structure of a thin film. The main advantage in comparison with the scanning tunneling and atomic force microscopies is the ability to trace also the inner and buried interfaces. A schematic view of the X-ray scattering techniques based on grazing incidence is given in Fig. 1.

This contribution is devoted to the surface and interface characterization by the X-ray specular reflectivity and diffuse scattering measurements at grazing incidence. The interface quality plays a dominant role in the thin film structures the operation of which is based on the interface phenomena like X-UV optical elements or metallic multilayers with antiferromagnetic coupling exhibiting the giant magnetoresistance effect.

2 Specular reflectivity of a single interface

The refractive index in the X-UV region is a complex quantity with the absolute value less than unity since the electronic transitions (resonant effects) start to be excited in the atoms:

$$n = 1 - \delta - i\beta \tag{1}$$

The decrements of the refractive index δ and β are connected with the real and imaginary parts of the atomic scattering factor, respectively, so that this expression relates the macroscopic quantity dependent on the electronic density (refractive index) to the atomic characteristics. In the absorption-free case below a critical angle of incidence θ_c

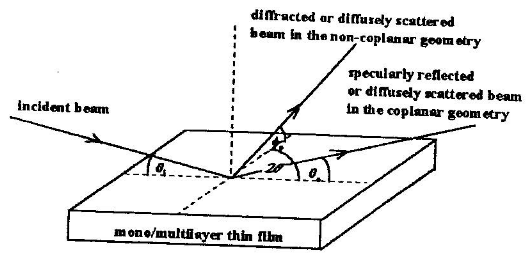

Fig. 1. Schematical view of the X-ray techniques based on grazing incidence. For $\theta_i = \theta_o$ and $\theta_i \neq \theta_o$, the specular reflectivity and diffuse (non-specular) scattering, respectively, sensitive to the interface quality are measured, θ_i and θ_o being tuned close to the critical angle for the total external reflection. For large θ_o, the diffraction sensitive to the atomic structure of a thin film is measured, the diffraction angle θ being half of that between the primary and secondary beams which is $\theta_i + \theta_o$ in the coplanar geometry. In the non-coplanar geometry, both θ_i and ϕ_o are close to the critical angle and the diffraction due to the in-plane periodicity, typical for epitaxial thin films, is measured. Alternatively, the diffuse scattering coming from amorphous atomic structure (for $2\theta >\approx 20°$) or rough interfaces (for $2\theta <\approx 20°$) is measured. The latter geometry was utilized in multilayer studies by Salditt et al. [11].

given as

$$\sin\theta_c = \sqrt{2\delta} \tag{2}$$

(measured with respect to the surface), the refractive angle is purely imaginary and only an evanescent wave at the depth of ≈ 4 nm is trapped in the material. Above θ_c, the refractive angle is purely real and the radiation starts to penetrate inside. In presence of absorption, the refractive angle is fully complex and the transition from predominantly imaginary to predominantly real values at θ_c is smeared.

The amplitudes of the specularly reflected and transmitted X-ray waves at an interface (related to the incident amplitude) may be derived from the boundary conditions of the electromagnetic field at the interface using the Maxwell equations which are the basis for the dynamical approach to the X-ray scattering. This procedure leads to the Fresnel coefficients known also from the optics of visible light. Neglecting absorption, the Fresnel reflection coefficient is constant and equal to unity below θ_c while the transmission coefficient increases from zero at the angle of incidence $\theta_i = 0$ up to the value of two at $\theta_i = \theta_c$ which is due to the constructive interference between the reflected and transmitted waves. Above θ_c, the reflection and transmission coefficients approach quickly to zero and unity, respectively. The measured specular reflectivity is the squared absolute value of the generally complex Fresnel reflection coefficient. In the absorption-free case, the reflectivity is equal to unity below θ_c while it decreases above θ_c, for $\theta_i >\approx 3\theta_c$ proportionally to $\frac{1}{\sin^4\theta_i}$. In practice, the break point at θ_c is "rounded" by absorption. The shape of the theoretical reflectivity curve for sapphire is

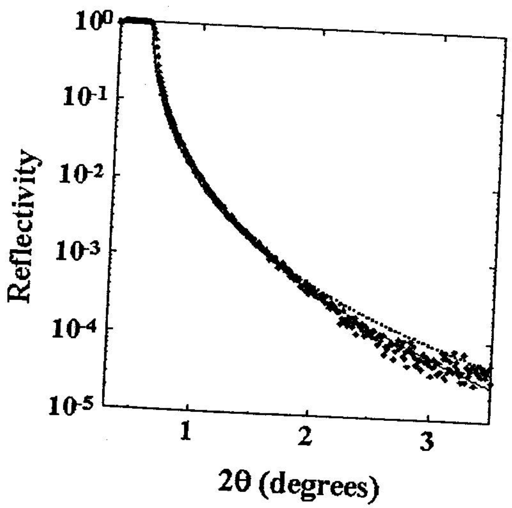

Fig. 2. Specular reflectivity calculated for a perfectly smooth sapphire surface (broken line) compared with that of the real surface simulated by Fresnel algorithm with a 0.3 nm interface roughness (line — simulation, dots — experimental points). 2θ is the angle between the primary beam and the observation direction (detector).

shown in Fig. 2.

An equivalent possibility to calculate the X-ray specular reflectivity is to use the wave equation

$$(\Delta + K^2) = V(r)E(r), \tag{3}$$

usually supposing the plane wave (Fraunhoffer approximation), where K is the wavevector length in vacuum, $E(r)$ is the amplitude, and $V(r)$ is set equal to the scattering potential of the ideal surface, $V(r) = V_{id}(r)$.

A real interface may be compositionally graded and/or geometrically rough which causes a depletion of the specularly reflected amplitude and a more rapid decrease of the specular reflectivity with θ_i than in the ideal case. As the scattering vector $\vec{q} = \vec{k}_2 - \vec{k}_1$ is kept perpendicular to the interface during a specular reflectivity measurement, $\vec{k}_1$ and $\vec{k}_2$ being the wavevectors of the incident and scattered waves, respectively, the attenuation of the ideal reflectivity depends only on the interface profile projection (represented e.g. by a change of the dielectric susceptibility) into the direction perpendicular to the interface. Most frequently, this interface profile is supposed to be described by the em error function as it is known from the diffusion theory. In this case, a Debye-Waller-like attenuation factor $e^{-q_1 q_2 \sigma^2}$ modifies the ideal reflectivity where q_1 and q_2 are the scattering vector lengths above and below the interface, respectively, and σ is the root-mean-square (rms) value of the Gaussian derivative of the interface profile called interface roughness. This attenuation factor was firstly derived within the dynamical approach to the X-ray scattering by Névot and Croce [1] and later confirmed within the distorted-wave Born approximation (DWBA - see below) by Sinha et al. [2]. In the Born approximation (BA - see below), both q_1 and q_2 are replaced by the scattering vector in vacuum. An example of the reflectivity simulation for a real sapphire surface is shown in Fig. 2. It may be seen that the interface roughness accelerates the reflectivity decrease comparing with the ideal curve.

3 Specular reflectivity of a multilayer

An extension of the reflectivity calculation from a single interface to a set of interfaces is quite straightforward using the Ewald formalism of the dynamical theory of the X-ray scattering. One starts at the ML/substrate interface and calculates backward the reflected amplitude at individual interfaces up to the surface using the recursive formula

$$A_{j,j+1} = a_j^4 \frac{A_{j+1,j+2} + r_{j,j+1}}{A_{j+1,j+2} r_{j,j+1} + 1} \tag{4}$$

where indexing starts at the surface, r_j is the Fresnel reflection coefficient and a_j is related to the wave phase shift between the $(j+1)$ th and j th interfaces. Formula (3) was firstly derived by Parratt [3] for a multilayer with ideal interfaces. For a real multilayer, a more general formula including the transmission coefficients is applicable

$$A_{j,j+1} = a_j^4 (r_{j,j+1} + \frac{A_{j+1,j+2} t_{j,j+1} t_{j+1,j}}{A_{j+1,j+2} r_{j,j+1} + 1}) \tag{5}$$

where Fresnel coefficients may be multiplied by the corresponding attenuation factors to include the interface roughness at each interface. If both reflection and transmission coefficients are multiplied, there is a depletion both of the reflected and transmitted amplitudes which is the case of geometrically rough interfaces. The attenuation of the reflected amplitude only corresponds to interdiffused interfaces where a decrease of the reflectivity is accompanied by an increased transmitivity and may be compensated for by the reflection from deeper interfaces. Due to the finite number of layers, the compensation effect vanishes with increasing θ_i so that the biggest difference between the two interface cases is close to θ_c. The Debye-Waller-like attenuation factors decrease the amplitude of the ideal reflectivity modulations discussed below but do not affect their widths. Layer thickness fluctuations, which can easily be incorporated into the calculation, cause both the lowering and broadening of the reflectivity modulations.

The matrix approach proposed by Abelès [4] offers a more effective calculation. Here, each layer is described by a transfer matrix, connecting the fields above and below the interface, and the total reflected amplitude is obtained in one step by multiplication of all interface matrices.

In the case of periodic multilayers, a "crystallographic" approach relying on an analytical formula may accelerate the reflectivity calculation. In this case, a multilayer is viewed as a one-dimensional crystal and the amplitudes from individual atoms (over unit area) are summed up as in traditional crystals. Henke [5] implemented the Darwin-Prins dynamical scattering model while Fullerton et al. [6] applied a formula

$$I(q) = L(q)|F(q)|^2 \tag{6}$$

where $L(q)$ is the Laue function corresponding to the multilayer periodicity and $F(q)$ is the kinematical structure factor of the basic motif ("unit cell") of the multilayer stack. Neither of these approaches reproduces the TER region. Due to the limited thickness, multilayers often behave kinematically from rather low θ_i values when the kinematical approach is sufficient. The interface roughness in "crystallographic" kinematical approach is incorporated by averaging the resulting formula over Gaussian distribution of the individual layer positions. This distribution may be discrete (e.g. for strongly textured multilayers) or continuous (e.g. for amorphous multilayers). If the fluctuations in one layer affect the fluctuations in the above lying ones, which is the most realistic case, a cumulative layer disorder is established. In this case, the averaging causes both a decrease of the amplitude and an increase of the width of the ideal reflectivity modulations.

4 Evaluation of the specular reflectivity

An example of the specular reflectivity curve measured on a periodic W/Si multilayer composed from amorphous layers is shown in Fig. 3. Due to the interference effects, the reflectivity curve is no more smooth. There are two kinds of maxima. The large ones are the Bragg maxima coming from the constructive interferences on the multilayer period d and obeying the Bragg equation corrected for refraction:

$$k\lambda = 2d\sqrt{|n|^2 - cos\theta_i{}^2} \tag{7}$$

where k is the Bragg order and n is the mean refractive index of the multilayer. Smaller maxima between the Bragg ones are the Kiessig fringes due to the interference of the waves reflected from the air/multilayer and multilayer/substrate interfaces, their positions being governed by a similar equation.

The most exhaustive evaluation of the reflectivity curve is provided by a simulation based on some of the previously described algorithms. The simulation gives the basic structural parameters, namely the individual layer thicknesses, the multilayer period and its repetition number, the total multilayer thickness, and the interface roughness. Alternatively, the decrements of the refractive index may be refined and thereby the electronic and atomic densities determined which may be different from the bulk values. This determination is possible rather independently of the determination of the interface roughness since δ and β control θ_c while σ controls the reflectivity decrease above θ_c. A reflectivity simulation based on the recursive method for the given W/Si multilayer is shown in Fig. 3., too.

For periodic multilayers even without a simulation, one can judge the quality and calculate some basic parameters directly from the reflectivity curve. Any deviation from the ideal multilayer periodicity causes also an irregularity of the reflectivity modulations. A mean multilayer period can be calculated from the positions of the Bragg maxima

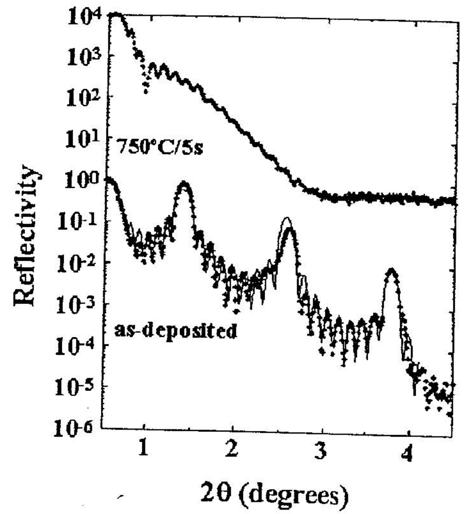

Fig. 3. Specular reflectivity of the 9 × (5 nm Si/1 nm W) amorphous multilayer deposited on the Si(100) wafer simulated by the Fresnel recursive formula (line — simulation, dots — experimental points). After the rapid thermal annealing at 750°C for 5s, the large Bragg maxima disappeared due to the interdiffusion/mixing at the interfaces and the oscillations typical for a monolayer thin film persist originating from the interferences of the waves reflected at the air/multilayer and multilayer/substrate interfaces. Their envelope is slightly wavy by the remaining concentration modulation across the collapsed multilayer. For further details see Ref. [7].

using Eq. (7) or some of its simplified versions. Similarly, the multilayer thickness can be calculated quite independently and thus the number of periods may be found or verified.

The reflectivity measurements have found an unprecedented application in the determination of very low interdiffusion coefficients up to the order of 10^{-27} m^2 s^{-1}. Within the kinematical approximation, the integrated intensity of the k-th order Bragg maximum is directly proportional to the amplitude of the k-th Fourier component of the compositional profile across the multilayer stack. The interdiffusion coefficient is determined from the temporal decrease of the integrated intensity of a Bragg maximum during an isothermal annealing which reflects a decay of the corresponding compositional wave component.

Generally, any thermal treatment leads to a degradation of the interfaces after some time. Such a collapse of the multilayer is also shown in Fig. 3. Therefore, thermal stability limits have to be known precisely for any multilayer application with an increased thermal loading like those in the intense plasma source diagnostics or synchrotron radiation optics. For further details of the measurements and simulations presented in Fig.

3. see [7].

5 Interface diffuse scattering

At grazing incidence, the X-rays scattered on a surface or a layered thin film into non-specular directions are due solely to geometrical roughness of the interfaces. As their phase relation with respect to the incoming wave is random, they cannot interfere constructively and are distributed over the whole solid angle including the specular direction (diffuse or incoherent scattering). As explained above, a specular reflectivity measurement cannot distinguish between geometrically rough and compositionally graded interfaces. The diffuse scattering at grazing incidence provides a tool to study the real interface roughness and conformality of the interface profiles across a multilayer stack established during the growth.

The calculation of the diffuse scattering from a single rough interface or surface starts with the wave equation (3) which is solved iteratively. One possibility is to start with the solution in vacuum ($V(r) = 0$) and to obtain a vacuum plane wave . The differential scattering cross section in the first iteration (the first BA) may be then calculated as $d\sigma = |\langle E^{(2)}_{vac}|V|E^{(1)}_{vac}\rangle|^2 d\Omega$. This approximation does not include the multiple scattering processes and is applicable in most cases for $\theta_i >\approx 5\theta_c$ where the reflectivity drops to low values and the interaction of X- rays with matter is weak. This is the basis for the kinematical theory of the X-ray scattering.

Another possibility is to divide the scattering potential $V(r)$ into the undisturbed part representing the ideal perfectly smooth surface $V_{id}(r)$ and the disturbed part representing any deviation from the ideal planar shape $V_d(r)$ (the interface roughness). In this case, the solution for $V_{id}(r)$ gives the Fresnel coefficients, as stated above, while the differential scattering cross section in the first iteration (the first DWBA) is split into the coherent and incoherent (diffuse) parts. The coherent part corresponds to the specular reflectivity attenuated by the interface roughness, that may be calculated more effectively using the approach of the attenuation factors mentioned above, while the incoherent part is given by the covariance of the matrix element of the disturbance potential $V_d(r)$ in the basis of the eigenstates of the ideal scattering potential $V_{id}(r)$. Therefore, the DWBA is applicable for $\theta_i <$ (3-5) θ_c where the Fresnel states still represent a good description of the system. At larger θ_i, the BA is convenient. The BA and DWBA were used for the first time to treat the X-ray scattering from a rough surface by Sinha et al. [2].

The crucial point in the DWBA calculation is the description of the disturbance potential which requires the description of the interface morphology. For the random interface roughness, a statistical description by a self-correlation function is used which for many self- affine isotropic solid-state interfaces with cut-off exhibiting Gaussian roughness takes up the form

$$C(r) = \sigma^2 \exp\left(-(\frac{r}{\xi})^{2h}\right) \qquad (8)$$

where ξ is the lateral (along the interfaces) correlation length and $h \in \langle 0, 1\rangle$ is the fractal parameter connected with the fractal dimension of the interface as $D = 3 - h$. For $h = 1$, the fractal and topological dimensions are the same and there is no fractal behaviour of the interface, for $h = 0$, the fractal behaviour is at maximum. The cut-off takes into account the fact that a real interface is never a true self-affine one as it scales differently in the lateral and normal directions (the interface roughness is always limited).

An extension of the DWBA to the multilayer case was done by Holý et al. [8] for vertically non-correlated interface roughness. A more realistic case of conformal interfaces was treated by Holý and Baumbach [9]. Here, the conformality of the interface profiles (vertical interface roughness correlation) was also included into the expression of the disturbance potential by a vertical correlation function.

The interface roughness during a multilayer growth is predominantly governed by a complex interplay between the surface migration of the adatoms and the interfacial reaction in which they are involved, i.e. by a competition of the kinetic and thermodynamic parameters. Generally, an interface profile mimics to some extent the underlying interface and simultaneously takes up a vertically non-correlated roughness due to the fluctuations in the adatom flux during the deposition:

$$\Delta z_j(r) = \Delta z_{j+1}(r) * a_j + \acute{\Delta} z^{int}(r). \qquad (9)$$

Here, $\Delta z_j(r)$ is a normal deviation from the ideally smooth reference j th interface, $a_j(r)$ is a replication factor, and $z_{int}(r)$ corresponds to the intrinsic non-correlated part of the interface roughness, the indexing starting from the surface. The replication factor is related to the vertical correlation function and may be determined from a microscopic layer growth model like that of Kardar, Parisi, and Zhang [10] (KPZ). At the stationary growth conditions, all interfaces possess the same lateral correlation function and the vertical correlation function is expressed as its attenuation across the multilayer, in the KPZ model as

$$L(q_x, z_j - z_k) = \exp\left(-\frac{q_x^2|z_j - z_k|}{\alpha}\right) \qquad (10)$$

Here, q_x is the lateral component of the scattering vector, z_j and z_k are the mean positions of the j th and k th interfaces, and α controls the degree of the vertical interface correlation ($\alpha \to \infty \Rightarrow$ total correlation, $\alpha = 0 \Rightarrow$ no correlation). In this model, the vertical replication between the j th and k th interfaces at a given α decreases with increasing frequency of the interface roughness component corresponding to an increasing lateral component of the wavevector transfer q_x. This is due to the fact that the adatom surface migration during the deposition breaks predominantly the vertical correlation of the higher-frequency components of the Fouries series representing the interface roughness which are manifested further from the specular direction. A phenomenological vertical correlation function independent of the interface roughness frequency with the attenuation function

$$L(z_j - z_k) = \exp\left(-\frac{|z_j - z_k|}{L_{vert}}\right) \qquad (11)$$

may describe better the experimental results in some cases, L_{vert} being the vertical correlation length. Analogous correlation length stemming from Eq. (10) $L_{vert} = \alpha/q_x^2$ is frequency dependent.

In the case of the non-coplanar geometry, it is possible to determine both the lateral and vertical correlation lengths as well as the fractal parameter of the interfaces from the asymptotic behaviour of a multilayer Bragg maximum parameters with increasing out- of-plane component of the scattering vector as it was shown by Salditt et al. [11]. This approach overcomes the ignorance of the precise form of a real correlation function.

6 Measurements of the interface diffuse scattering

The distribution of the diffuse scattering coming from rough interfaces in the reciprocal space along and perpendicularly to the interfaces is fully determined by the lateral and vertical interface roughness correlations, respectively. Therefore, all basic interface parameters, related to the mechanism of the deposition process, may be obtained from a proper simulation of the experimental curves. These parameters include the lateral and vertical correlation lengths, fractal interface parameter, and rms value of the geometrical interface roughness including its development across the multilayer according to the model of the interface conformality used. For example in the KPZ growth model, the surface diffusion of adatoms is considerably limited by the interfacial reaction which results into interface roughening and interface roughness rather independent of the multilayer period. In the case of zero surface diffusion, the interface roughness increases toward the surface as

$$\sigma_j = \sqrt{\sigma_N^2 + (N-j)\Delta\sigma^2} \qquad (12)$$

where N is the total number of interfaces and $\Delta\,\sigma$ is the intrinsic non-correlated part of the interface roughness. In this case, the interface profiles are perfectly replicated but not identical.

In the case of the vertical interface conformality, the distribution of the diffuse scattering intensity in the reciprocal space is not quite uniform but it is concentrated into the stripes around the Bragg points (Fig. 4.). They originate from the constructive interferences of the diffusely scattered waves on conformal interfaces (resonant diffuse scattering - RDS). In the case of non-correlated interfaces, the distribution of the diffusely scattered X-rays throughout the reciprocal space is monotonous.

The diffuse scattering distribution in the reciprocal space may be measured in any geometry with a non-zero lateral component of the scattering vector. Detector (sample) scans with the fixed sample (detector) and rotating detector (sample) may be used in the coplanar geometry. Alternatively, an offset from the specular position is used before starting the measurement in the reflectivity mode (offset scan). The corresponding trajectories in the reciprocal space are shown in Fig. 4. The non-coplanar geometry enables us to increase the lateral component of the scattering vector by more than one order of magnitude [11].

An example of the diffuse scattering measurements on amorphous W/Si multilayers is shown in Fig. 5. (sample scans) and Fig. 6 (detector scans). These refractory

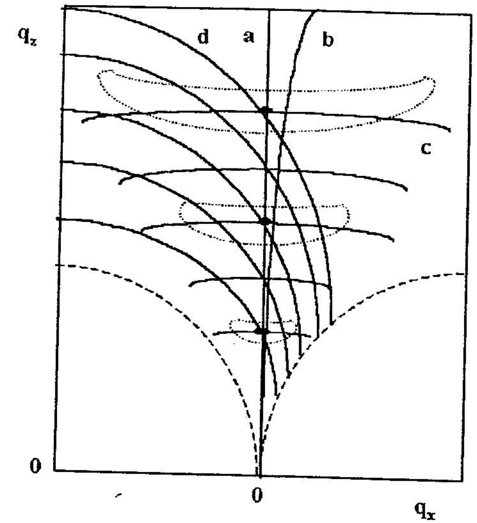

Fig. 4. Trajectories of different scans in the reciprocal space: a — specular reflectivity scan, b — offset scan, c — sample scans, d — detector scans; q_x and q_z being the lateral and normal components of the scattering vector, respectively. The black points are the multilayer Bragg maxima. The concentration stripes of the resonant diffuse scattering (RDS) around the Bragg maxima are shown by the dotted lines. They are curved at the extremities due to the refraction. The limiting Ewald spheres (broken lines) divide the reciprocal space into the accessible and inaccessible parts for the reflection geometry.

metal/metalloid multilayers with a high contrast of electronic densities are promising candidates for the X-UV optical elements. Three different samples were deposited simultaneously by electron-beam evaporation at different angles with respect to the sample normal. The intention of the oblique deposition was to achieve smoother interfaces and thus increase specular reflectivity. In the sample scans measured with the detector fixed at a Bragg order (Fig. 5), there is a central specular maximum, broadened by the multilayer mosaicity and experimental resolution, which is superimposed on a broader background due to the interface diffuse scattering. Additional S-shaped maxima occur on this background when θ_i (or the angle of exit) is equal to a Bragg angle and a standing wave field in the multilayer is established. The intensity of the broad background is most pronounced for the normal deposition and decreases by one order of magnitude with increasing deposition angle (more oblique deposition). In the detector scans (Fig. 6.), there is always a strong specular maximum and the additional ones which also disappear with more oblique deposition. These additional maxima as well as an increased broad background in the sample scans result from the intersection of the corresponding scan trajectory with the stripes of the RDS in the reciprocal space (see Fig. 4.) so that their disappearance gives a direct evidence of a loss of the vertical

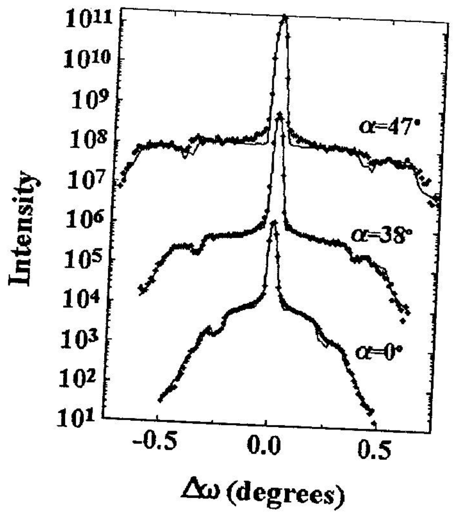

Fig. 5. Sample scans measured around the 2nd Bragg maximum on the amorphous W/Si multilayers deposited simultaneously at different angles α with respect to the surface normal as indicated in the figure. For $\alpha = 0°$, the multilayer is described as $10 \times$ (13 nm Si/2 nm W), the thicknesses of other ones are modified according to $\cos\alpha$. A gradual loss of conformality with increasing deposition angle is evidenced by decreasing background coming from the RDS. The curves were simulated within the DWBA and Kardar-Parisi-Zhang (KPZ) model of the vertical interface conformality (line — simulation, dots — experimental points). For further details see Ref. [12].

interface conformality with increasing deposition angle.

The DWBA simulations based on the vertical correlation function following from the KPZ growth model, Eq. (10), are shown in Fig. 5. and Fig. 6, too. The lateral correlation length decreases from 24 nm for the normal deposition up to 2.5 nm for the most oblique deposition and the parameter controlling the vertical interface conformality decreases from 0.02 nm $^{-1}$ to nearly zero. For $\alpha = 0.02$ nm $^{-1}$ and the roughness frequency corresponding to the lateral wavevector transfer at the extremities of the sample scan around the 2nd Bragg maximum, the vertical correlation length is of the order of the multilayer thickness. This means that for normally deposited sample, the interface roughness is fully replicated nearly in the whole interval of the frequencies sampled by the scans while the most oblique deposition practically destroys the vertical interface conformality which is accompanied also by a decrease of the lateral correlation length by one order of magnitude. No fractal behaviour of the interfaces was detected ($h = 1$). A striking result of the oblique deposition, owing to the expectation, is an increase of the rms value of the stationary interface roughness σ from 0.95 nm to 1.1 nm. Contrary to that from the specular reflectivity, this is a "true" geometrical roughness for which the "reflectivity roughness" is a starting estimate only. The roughness increase means that an increased lateral component of the adatom mobility during the oblique deposition provides an enhanced transport of the deposited material particles to a limited number of thin film nucleation centres thus promoting the formation of hills rather than to erode hills and fill valleys as it was expected.

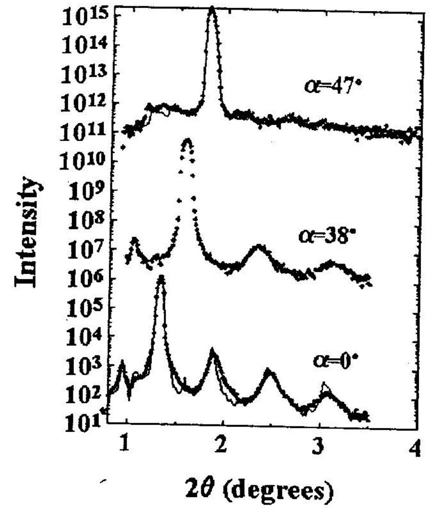

Fig. 6. The detector scans measured through the 2nd Bragg maximum on the same W/Si multilayers as in Fig. 5. The non-specular maxima come from the intersection of the scan trajectory in reciprocal space with the stripes of the RDS. Their disappearance with increasing deposition angle is consistent with a gradual loss of the vertical interface conformality concluded from Fig. 5. For further details see Ref. [12].

From the application point of view, an increased interface roughness leads to a lower specular reflectivity while the diffuse scattering deteriorates the contrast for imaging, especially when the interface profiles are conformal and the diffuse intensity close to Bragg maxima increases. In our case, the latter effect is much more distinct and important than the former one. Therefore, there is a merit of the oblique deposition for the W/Si multilayer elements for imaging devices but not for the elements where the specular reflectivity is important (monochromators, band-pass filters...). Further details of the oblique deposition study may be found in [12].

7 Conclusions

This paper outlined the utilization of the hard X- ray reflectivity and diffuse scattering at grazing incidence for the surface/interface characterization of thin films. After a general introduction to the topic, we have demonstrated on some practical examples how it is possible to obtain the basic parameters of mono/multilayer thin films including the surface/interface characteristics provided a proper description of the scattering process is combined with a proper surface/interface description and a model of the vertical interface conformality which reflects the growth mechanism during the deposition.

The techniques discussed are complementary to the grazing-incidence X-ray diffraction techniques for characterization of the internal structure of thin films which were not treated here. Comparing with well established traditional X-ray diffraction techniques for bulk materials, the X-ray techniques based on grazing incidence still experience a rapid development, both theoretical and experimental. At present, this progress is tightly connected with synchrotron storage rings of the 4th generation producing highly intense, coherent and polarized synchrotron radiation in a broad energy range from the far infrared to gamma region. Here, new types of grazing-incidence experiments profiting from unique properties of the synchrotron radiation have been devised, often connected with the development of new X-UV optical elements to bring conveniently processed synchrotron light from the ring to an experiment.

Acknowledgements This work was partly supported by the Slovak Grant Agency (VEGA), project No. 5083/98, and Ministry of Education of Czech Republic, project No. VS 96 102.

References

[1] L. Névot, P. Croce: *Rev. Phys. Appl.* **15** (1980) 761
[2] S.K. Sinha, E.B. Sirota S. Garoff, H.B. Stanley: *Phys. Rev.* **B 38** (1988) 2297
[3] L.G. Parratt: *Phys. Rev.* **95** (1954) 359
[4] F. Abelès: *Ann. Physique* **5** (1950) 596
[5] B.L. Henke: *J. X-ray Sci. & Technology* **2** (1990) 17
[6] E.E. Fullerton, I.K. Schuller, H. Vanderstraeten, Y. Bruynseraede: *Phys. Rev.* **B 45** (1992) 9292
[7] M. Jergel, V. Holý, E. Majková, Š. Luby, R. Senderák: *J. Appl. Crystallography* **30** (1997) 642
[8] V. Holý, J. Kuběna, I. Ohlídal, K. Lischka, W. Plotz: *Phys. Rev.* **B 47** (1993) 15896
[9] V. Holý, T. Baumbach: *Phys. Rev.* **B 49** (1994) 10668
[10] M. Kardar, G. Parisi, Y.C. Zhang: *Phys. Rev. Lett.* **56** (1986) 869
[11] T. Salditt, T. Lott, T.H. Metzger, J. Peisl, G. Vignaud, P. Høghøj, O. Schärpf, P. Hinze, R. Lauer: *Phys. Rev.* **B 54** (1996) 5860
[12] M. Jergel, V. Holý, E. Majková, Š. Luby, R. Senderák: *J. Phys. D Appl. Phys.* **28** (1995) A241